In Situ SHINERS at Electrochemical Single-Crystal Electrode/Electrolyte Interfaces: Tuning Preparation Strategies and Selected Applications

Jian-Feng Li,[†,§] Alexander Rudnev,[†,‡,§] Yongchun Fu,[†] Nataraju Bodappa,[†] and Thomas Wandlowski[†,*]

[†]Department of Chemistry and Biochemistry, University of Bern, Freiestrasse 3, Bern, Bern CH-3012, Switzerland and [‡]Frumkin Institute of Physical Chemistry and Electrochemistry, Russian Academy of Sciences, Leninskii pr. 31, Moscow, Moscow Oblast 119991, Russia. [§]J.-F. Li and A. Rudnev contributed equally to this work

ABSTRACT We have studied Au(55 nm)@SiO_2 nanoparticles (NPs) on two low-index phases of gold and platinum single crystal electrodes in ClO_4^- and SO_4^{2-} ion-containing electrolytes by both electrochemical methods and *in-situ* shell-isolated nanoparticle enhanced Raman spectroscopy (SHINERS). We showed the blocking of the electrode with surfactants originating from the synthesis of as-prepared SHINERS NPs. We introduce an efficient procedure to overcome this problem, which provides a fundamental platform for the application of SHINERS in surface electrochemistry and beyond. Our method is based on a hydrogen evolution treatment of the SHINERS-NP-modified single-crystal surfaces. The reliability of our preparation strategy is demonstrated in electrochemical SHINERS experiments on the potential-controlled adsorption and phase formation of pyridine on Au(hkl) and Pt(hkl). We obtained high-quality Raman spectra on these well-defined and structurally carefully characterized single-crystal surfaces. The analysis of the characteristic A_1 vibrational modes revealed perfect agreement with the interpretation of single-crystal voltammetric and chronoamperometric experiments. Our study demonstrates that the SHINERS protocol developed in this work qualifies this Raman method as a pioneering approach with unique opportunities for *in situ* structure and reactivity studies at well-defined electrochemical solid/liquid interfaces.

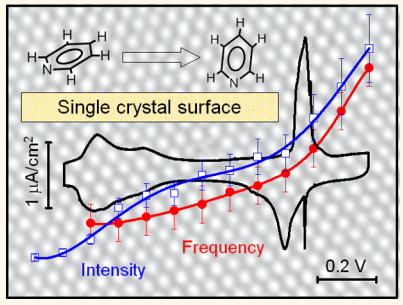

KEYWORDS: single-crystal electrodes · surface-enhanced Raman · SHINERS · Au@SiO_2 · nanoparticles · cyclic voltammetry · pyridine

Surface enhanced Raman spectroscopy is a powerful spectroscopic technique to study molecular adsorption and mechanisms of electrochemical reactions at metal/electrolyte interfaces.[1−3] The method was initially limited to rough and/or nanostructured surfaces of coinage metals and subsequently extended toward transition metals by exploiting various concepts of "borrowing" SERS activity.[4−6] During the past decade, template and nanoparticle-based fabrication strategies led to various SERS-active plasmonic nanostructures of controlled size, shape and composition to approach single molecule sensitivity and to overcome the problem of ill-defined surface morphologies of roughened samples.[7,8] Examples for applications at electrochemical solid/liquid interfaces are gold and silver nanoclusters,[9−11] nanorods[12] and template-based or nanosphere lithography.[13,14]

The extension of SERS to well-defined single-crystal metal/electrolyte interfaces was pioneered by Otto *et al.*, who studied the adsorption of pyridine molecules on Cu(hkl) surfaces.[15] Ikeda *et al.*[16] and Cui *et al.*[17] reported high quality, potential-dependent Raman spectra of aromatic thioles on gold single-crystal electrodes using gap-mode plasmon excitation in a sandwich structure Au(hkl)/organic monolayer/Au(55 nm) nanoparticles (NPs). A particular unique approach for expanding SERS to electrified single-crystal electrode/electrolyte interfaces, termed shell-isolated nanoparticle enhanced Raman spectroscopy (SHINERS), was developed by Tian *et al.*[18−21] The principle of the method is based on the assembly of a sphere-plane gap mode system composed of gold or silver NPs surrounded by a chemically inert, ultrathin and pinhole-free coating of SiO_2 or Al_2O_3, dispersed on electrode surfaces, such as metals, oxides or silicon. The NPs act as plasmonic antennas and provide the electromagnetic

* Address correspondence to thomas.wandlowski@dcb.unibe.ch.

Received for review July 7, 2013 and accepted September 5, 2013.

Published online September 05, 2013
10.1021/nn403444j

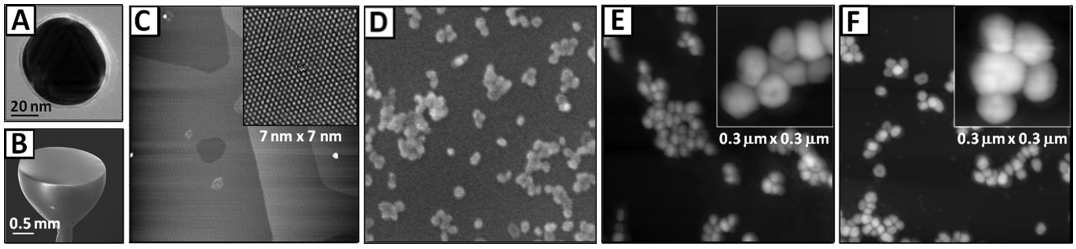

Figure 1. (A) HRTEM image of 55 nm Au@SiO_2 NPs with ~3 nm shell thickness. (B) SEM image of a Au(111) half-bead single-crystal electrode. (C) Large-scale AFM and high-resolution (7 nm × 7 nm) STM images of an island-free Au(111)-(1 × 1) surface. (D) SEM image and (E,F) AFM images of a Au(111)-(1 × 1) single-crystal surfaces modified with Au@SiO_2 SHINERS NPs (E) before and (F) after HER cleaning procedure. The corresponding insets represent magnifications (0.3 μm × 0.3 μm) of SHINERS NP islands. The large scale images in panels (C) to (F) represent frames of (2 μm × 2 μm) in size.

enhancement of Raman scattering, while the SiO_2 or Al_2O_3 shells prevent the core from interacting with the electrochemical system under study. Three-dimensional finite-difference-time-domain (3D FTDT) simulations demonstrated that most of the enhancement occurs between the SHINERS NPs and the substrate.[18]

The overall SHINERS signal is substantially greater than for tip-enhanced Raman spectroscopy (TERS), an alternative plasmon-based approach for Raman spectroscopy at single-crystal surfaces with potential for applications in an electrochemical environment.[22,23] The latter is based on a single TERS tip, while the laser in the former approach probes a significantly larger number of plasmonic antennas.[18,19] SHINERS has been demonstrated to give high quality Raman spectra of adsorbates at various atomically flat surfaces, such as Au(hkl), Pt(hkl), Rh(hkl) and Cu(hkl). Examples include hydrogen on Pt(111)[18] and Rh(111),[19] CO on Pt(111),[19] SCN^- on Au(hkl),[18] pyridine on Au(hkl) and Pt(hkl),[20] viologen on Au(111),[24] 2,2′-bipyridine on Au(hkl),[25] benzotriazole on Cu(hkl)[26] and two very recent studies of Au(111) surface oxidation in H_2SO_4[27] respective alkynes on Pt(111).[28] These pioneering studies demonstrate convincingly the ability of SHINERS to obtain high-quality face-dependent Raman spectra of adsorbates at single-crystal surfaces. The method bears a great potential in exploring correlations between structure and reactivity as well as in monitoring intermediates and pathways for a wide range of fundamental and applied processes at electrochemical interfaces.

However, the more general application of SHINERS in surface electrochemistry requires several important issues to be addressed. These include (1) the modeling of the spectroscopic response, the role of adsorbates and nearby solution species, (2) exploring SHINERS NPs as plasmonic antennas "only" and minimizing their role on the spatial occupation (blocking) of surface sites, (3) the chemical inertness of the NP-shell as well as (4) their effect on the potential distribution at the modified electrode/electrolyte interface. The preparation of chemically inert and "clean" single-crystal surfaces modified with SHINERS NPs for subsequent structure and reactivity studies is rather difficult. Reagents used in the synthesis of the NPs may interfere severely with Raman signals of adsorbates under investigation. Attempts to improve the inertness of NPs involve iodine displacement,[29] chemical polishing with cyanide,[30,31] ozone cleaning,[32] argon ion sputtering[31] or the deposition of ligand-free NPs on suitable substrates in a vacuum.[13] However, none of these methods are applicable to single-crystal surfaces modified with SHINERS NPs because of surface roughening and damaging of the isolation shell.

In this paper we explore the influence of submonolayer coverages of Au(55 nm)@SiO_2 (~3 nm) NPs on the electrochemical response of low-index gold and platinum single-crystal electrodes (Figure 1A–C) in ClO_4^- and SO_4^{2-} ion-containing electrolytes. We address the blocking of surface sites and introduce cathodic polarization as a unique strategy to prepare electrochemically rather inert NP-modified electrode surfaces. The quality of this preparation strategy is illustrated in electrochemical SHINERS experiments on the potential-controlled adsorption and phase formation of pyridine on Au(hkl) and Pt(hkl).

RESULTS AND DISCUSSION

Electrochemical Conditioning of the Au(111)-Au(55 nm)@SiO_2 Electrodes. Figure 1D,E shows typical SEM and AFM images of a Au(111)-(1 × 1) surface modified with Au(55 nm)@SiO_2 SHINERS NPs. The sample was prepared by drop-casting a dilute NP solution followed by gentle drying in a stream of argon and subsequent extended rinsing with Mill-Q water to dissolve unbound particles. Following this protocol, we obtained submonolayers of NPs with coverages ranging between 20 to 30%. Typically, the NPs are assembled in evenly distributed small islands containing from 4 up to 30 NPs. These islands are rather uniformly distributed on the substrate surface under our experimental conditions. The statistical analysis demonstrates that the islands contain typically 15–20 NPs (see Supporting Information for details). Isolated NPs or three-dimensional clusters are rarely observed after HER treatment.

Cyclic voltammograms (CVs) recorded in the double layer regions as well as upon extension to surface oxidation and reduction demonstrate a distinct influence of

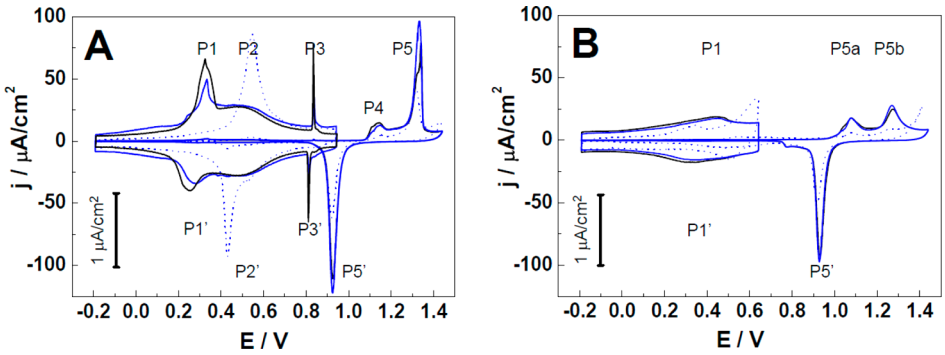

Figure 2. CVs of Au(111)-(1 × 1) single-crystal bead electrodes unmodified (black lines) and modified (solid blue lines) with Au@SiO_2 SHINERS NPs. The dotted blue traces were recorded with "as-prepared" NPs, while the solid blue lines represent data obtained with HER-SHINERS NPs. The voltammograms in the double layer region are displayed with a magnification factor of 30. Solution: 0.1 M (A) H_2SO_4 and (B) $HClO_4$. Scan rate: 10 mV/s.

the SHINERS NPs on the electrochemical response. As an example, Figure 2 displays the corresponding data for Au(111) in 0.1 M H_2SO_4 and 0.1 M $HClO_4$. The solid black lines represent the response of the unmodified, atomically flat Au(111) electrode, while the dotted blue curves are obtained in the presence of "as-prepared" SHINERS NPs following the procedure outlined in the literature[18,33] and summarized briefly in the Methods section. The double layer currents and the oxidation/reduction pattern are strongly distorted. The characteristic features in the charging current representing the lifting and reformation of the surface reconstruction Au(111)-(p × $\sqrt{3}$) → Au(111)-(1 × 1) (P1/P1′), the adsorption of sulfate ions (P2/P2′) and the transition into the ordered ($\sqrt{3}$ × $\sqrt{7}$) sulfate phase (P3/P3′)[27,34−39] are quenched for Au(111)/0.1 M H_2SO_4 in the presence of "as-deposited" NPs during both the anodic and the cathodic scans (Figure 2A). Extending the potential range up to 1.45 V demonstrates that the NPs diminish the Faraday charges representing the surface oxidation at step (P4) sites. The position of the reduction peak P5′ appears to be not influenced by the presence of the "as-prepared" SHINERS NPs (Figure 2A). However, the current magnitude is reduced. Inspection of the surface by AFM reveals that multiple cycling the potential in the double layer regions and upon oxidation/reduction does not modify the coverage of the SHINERS NPs.

Similar trends as for Au(111)/0.1 M H_2SO_4 were also observed in 0.1 M $HClO_4$ (Figure 2B). The weaker specific adsorption of ClO_4^- anions, as compared to SO_4^{2-}, leads to rather broad features for the lifting (P1) and reformation (P1′) of the surface reconstruction within the time scale of the voltammetric experiments. Oxide formation on terrace sites and the AuO place exchange take place on energetically different steps as represented by the occurrence of two current peaks labeled P5a and P5b.[38,39] Their exact nature is still not clear.

In conclusion, we may state that the as-prepared SHINERS NPs influence the double layer and the oxidation/reduction response of Au(111) in H_2SO_4 and in $HClO_4$ electrolytes severely. Possible reasons are blocking of surface sites or organic contaminants released from the NPs upon deposition and polarization.

In an attempt to overcome the undesired electrochemical response, we developed a protocol based on polarization in the hydrogen evolution range (HER) followed by sequences of electrolyte-exchange cycles. The Raman spectra were monitored simultaneously: An electrode (Au(hkl) or Pt(hkl)) modified with a submonolayer of SHINERS NPs was mounted in a three-electrode thin-layer cell (Au or Pt wires as counter electrodes, and Ag/AgCl as reference electrode) filled with deoxygenated neutral electrolyte, such as 0.1 M $NaClO_4$. We typically used a spectro-electrochemical cell in a vertical configuration (Figure 3A). A thin electrolyte film was established by positioning the working electrode close to the optical quartz window (less than 50 μm). Next, the electrode was polarized at −2.00 V *vs* Ag/AgCl for 50−100 s. The HER proceeds vigorously. However, the thin layer geometry prevents the formation of big hydrogen bubbles, which keeps the submonolayer of NPs rather stable. This polarization procedure was repeated 3 to 4 times, accompanied by cycles of solution exchange to remove the desorbed impurities.

The efficiency of the procedure is illustrated in the sequence of Raman spectra displayed in Figure 3B. *Trace a* was recorded at 0.00 V in 0.1 M $NaClO_4$ for Au(111) covered with 0.2 mL of Au(55 nm)@SiO_2 NPs. We observed broad peaks at ∼1308, ∼1565 and ∼2883 cm^{-1}, which are assigned to C−C, C═C and C−H vibration modes of adsorbed organics. Polarization at −2.00 V leads to the desorption of these species as indicated by the absence of the three bands in the SHINERS *trace b* of Figure 3B. The feature at 1618 cm^{-1} corresponds to the bending mode of interfacial water. Electrolyte exchange and several repetitions of the polarization at −2.00 V resulted in Raman spectra without any impurity contribution as illustrated by *trace c* in Figure 3B. The spectrum was recorded at 0.00 V. Comparison with *trace a* demonstrates the

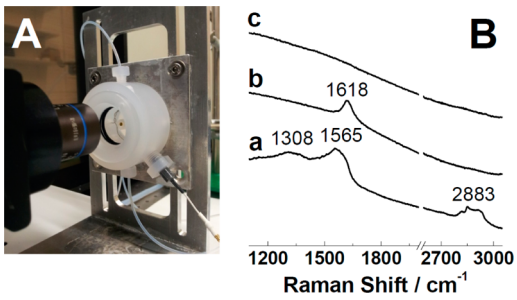

Figure 3. (A) Picture of the thin-layer electrochemical Raman cell employed for the HER-cleaning and the spectroscopic characterization. (B) SHINERS spectra of a Au(111) single-crystal electrode (a) before (E = 0.00 V), (b) during (E = −2.00 V), and (c) after (E = 0.0 V) the HER cleaning procedure in 0.1 M $NaClO_4$ solution.

efficiency of the HER-polarization and electrolyte exchange procedure. The SHINERS spectra plotted in Figure 3B are typical representations of properties of the entire NP-modified Au(111) surface. AFM inspection of the polarized Au(111) surface reveals a ~5% decrease of the NP coverage and a slight increase of the island size (Figure 1F). Finally, we also like to emphasize that the HER in *acidic electrolyte* does not lead to the complete removal of organic adsorbates, as monitored by *in situ* Raman experiments.

Employing the HER-treated Au(111) electrode in voltammetric experiments in 0.1 M H_2SO_4 or 0.1 M $HClO_4$ leads to curves (solid blue lines in Figure 2) that are almost identical to the response of the NP-free surface (black lines in Figure 2). The most pronounced difference is a 10% increase of the double layer charging current at $E < E$(P1), *i.e.*, at a negatively charged surface, and a *ca.* 10% reduction of the charge consumed during lifting/reformation of the surface reconstruction (P1/P1′), as well as of the disorder/order phase transition within the sulfate adlayer (P3/P3′ in Figure 2A). Position and charge of the characteristic current peaks of surface oxidation (P4, P5) and reduction (P5′) appear to be unaltered in both electrolytes.

We also performed control experiments with NP-free Au(111) electrodes. The HER-treatment following a similar protocol as described above does not change the shape of the current−voltage response. The double layer responses and the characteristics in the gold surface oxidation/reduction regions are identical to the black traces in Figure 2.

Cyclic Voltammograms of Au(100)-(1 × 1) in the Presence of SHINERS NPs. In an attempt to generalize the HER-treatment for preparing high-quality SHINERS-NP modified electrodes, we investigated next the electrochemical response of Au(100)-(1 × 1) electrodes in 0.1 M H_2SO_4 and 0.1 M $HClO_4$ (Figure 4). The Au(100)-(hex) reconstruction was lifted prior to the electrochemical experiments following a previously described protocol,[40] which gives rise to large, island-free terraces of several hundreds of nm^2 with a nominal quadratic arrangement of the gold surface atoms.[40] The coverage of the SHINERS NPs was estimated to approximately 20%. To eliminate possible interference with the potential-induced reformation of the Au(100)-(hex) surface reconstruction,[40,41] all experiments started at 0.60 V. The black and blue solid traces, which represent the current *vs* potential response of the bare and of the cleaned NP-modified Au(100)-(1 × 1) electrodes, are basically identical in the double layer region as well as upon extension toward surface oxidation/reduction in both electrolytes. The voltammograms reveal signatures of nearly perfect, defect-free Au(100)-(1 × 1) electrodes in both electrolytes.[38−40,42,43] P1, which is located at 0.34 V in H_2SO_4, and more positive at 0.57 V in $HClO_4$, represents the charge contributions due to the lifting of a small fraction of potential-induced Au(100)-(hex) reconstructed patches (<5%).

The current response in the surface oxidation/reduction regions reveals the characteristic current peaks P4 and P5 representing surface oxidation at step and terrace sites as well as a single cathodic reduction peak P5′. The corresponding charges of 640 $\mu C\ cm^{-2}$ (H_2SO_4) and 620 $\mu C\ cm^{-2}$ ($HClO_4$) decrease by less than 10% in the presence of the "cleaned" SHINERS NPs. AFM experiments demonstrated that the NP coverage is not changing during multiple oxidation/reduction cycles.

Finally, we notice in Figure 4 the distinct difference in the current response of Au(100)-(1 × 1) modified with HER-SHINERS (solid blue line) and "as-deposited" SHINERS NPs (dotted blue lines). This comparison illustrates the importance for establishing carefully designed and evaluated experimental protocols for SHINERS NPs on electrode surfaces to obtain meaningful electrochemical and Raman signatures on atomically smooth single-crystal electrode surfaces.

SHINERS NPs on Pt(111)-(1 × 1) and Pt(100)-(1 × 1). Next we adopted the HER-based SHINERS-NP post-treatment to Pt(111) and Pt(100) electrodes. The Pt(hkl) bead electrodes, as prepared by flame-annealing and subsequent cooling in Ar/H_2, revealed high quality voltammograms of low-defect surfaces (black lines in Figure 5), which agree with literature data.[34−37,44] The data for Pt(111)/0.1 M H_2SO_4 show at $E < 0.10$ V, a clear signature P1/P1′ of hydrogen adsorption on terrace sites. The charge in $-0.20\ V \le E \le 0.10$ V is estimated to 160 $\mu C\ cm^{-2}$. The additional small peaks at −0.13 and 0.02 V represent hydrogen adsorption on (110) and (100) step sites.[35−37] P2/P2′ at $E > 0.10$ V represents a disordered adlayer of sulfate anions, which undergoes a disorder/order phase transition at P3/P3′. The height and the shape of this pair of current peaks is a measure of the long-range order and cleanliness of the Pt(111) terrace sites.[45] P4/P4′ at more positive potentials is assigned to a structure transition within the ordered sulfate layer.[46] The voltammogram of a cleaned Pt(111) electrode modified with a submonolayer of SHINERS NPs reproduces nearly all features of the bare Pt(111)

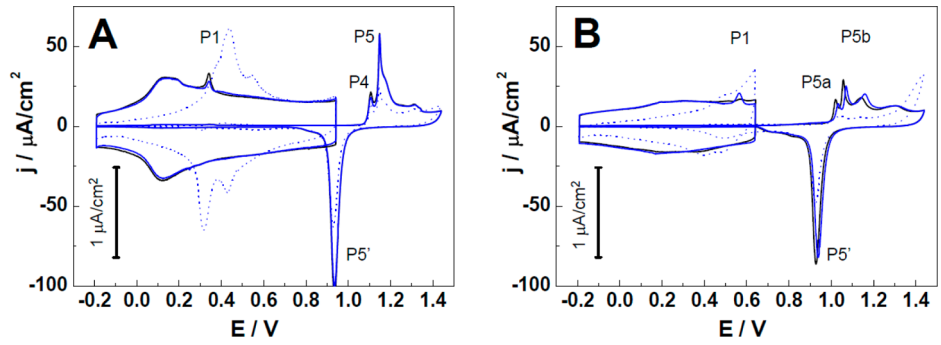

Figure 4. CVs of Au(100)-(1 × 1) single-crystal bead electrodes unmodified (black lines) and modified (solid blue lines) with Au@SiO_2 SHINERS NPs. The dotted blue traces were recorded with "as-prepared" NPs, while the solid blue lines represent data obtained with HER-SHINERS NPs. The voltammograms in the double layer region are displayed with a magnification factor of 30. Solution: 0.1 M (A) H_2SO_4 and (B) $HClO_4$. Scan rate: 10 mV/s.

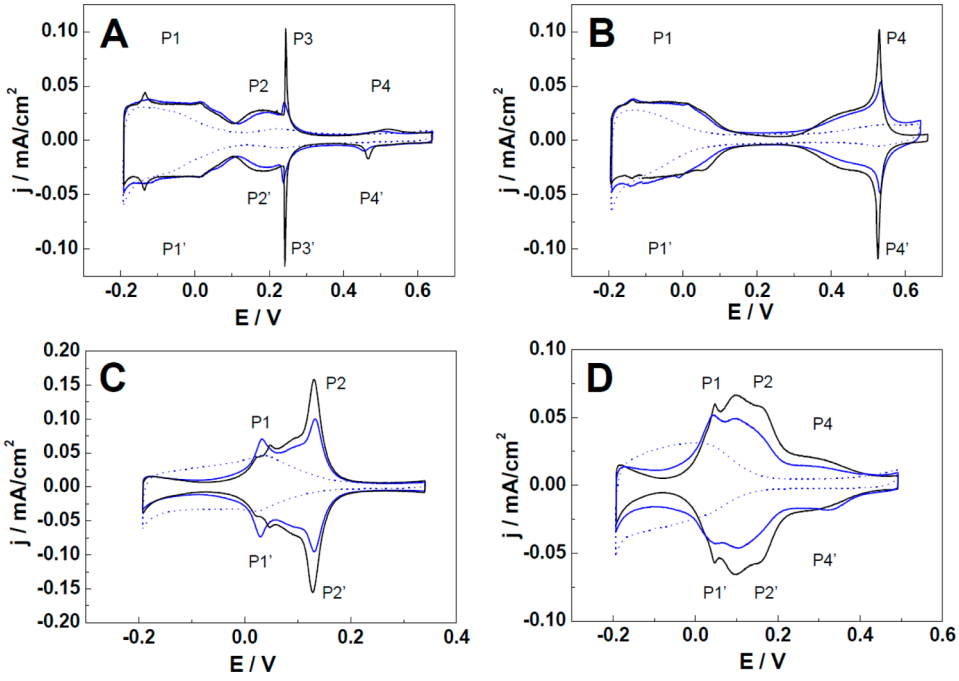

Figure 5. CVs of (A,B) Pt(111)-(1 × 1) and (C,D) Pt(100)-(1 × 1) single-crystal bead electrodes unmodified (black lines) and modified (solid blue lines) with Au@SiO_2 SHINERS NPs. The dotted blue traces were recorded with "as-prepared" NPs, while the solid blue lines represent data obtained with HER-SHINERS NPs. Solution: 0.1 M (A,C) H_2SO_4 and (B,D) $HClO_4$. Scan rate: 50 mV/s.

electrode in 0.1 M H_2SO_4. A comparison of the solid blue and black traces in Figure 5 reveals only a decrease of the charge consumed in P3/P3′ (<30%). On the other hand, experiments with "as prepared" SHINERS NPs lead to a significant depression of hydrogen adsorption until the onset of hydrogen evolution at $E < -0.20$ V, as well as to the blocking of sulfate and hydroxide adsorption at more positive potentials, which is indicated by the dotted blue line in Figure 5A.

Similar trends were observed for Pt(111) in 0.1 M $HClO_4$ (Figure 5B). The HER-SHINERS NPs do not alter the voltammogram for hydrogen adsorption (P1/P1′) and in the double layer charging region until $E \leq 0.30$ V. The charge consumed in -0.20 V $\leq E \leq 0.10$ V is estimated to 160 μC cm^{-2}. However, the so-called Butterfly peak P4/P4′ at $E > 0.30$ V, which is assigned to the reversible OH-adsorption,[47] decreases moderately in the presence of SHINERS NPs. The current response of the NP-modified Pt(111) electrodes without treatment by HER reveals the complete blocking of this region and a significant reduction of available (111) terrace sites in the potential region of hydrogen adsorption (dotted blue line in Figure 5B).

The situation is more complex for Pt(100)-(1 × 1) in 0.1 M H_2SO_4 and in 0.1 M $HClO_4$. The voltammogram of Pt(100)-(1 × 1) in 0.1 M H_2SO_4 (black line in Figure 5C) shows two characteristic current peaks labeled P1/P1′ at $E = 0.05$ V and P2/P2′ at $E = 0.13$ V. The latter is assigned to the adsorption/desorption of hydrogen and sulfate ions on (100) terrace sites, and the former to

that on (111) step and/or step-edge sites.[44,48−54] The total charge consumed in $-0.10\ V \le E \le 0.50\ V$ amounts to (220 ± 10) $\mu C\ cm^{-2}$. STM measurements demonstrated that Pt(100) electrodes, cooled down after flame-annealing in an Ar/H_2 atmosphere, are unreconstructed and composed of long and wide terraces, which alternate with step-bunched regions. On terraces wider than 500 nm, we also observed square-shaped Pt ad-islands of 0.21 nm height and 10 to 40 nm in $x-y$ dimensions.[44] This higher defect density, as compared to Pt(111)-(1 × 1), might explain why the HER-treatment of SHINERS-NP-modified Pt-(100) electrodes is less effective. The solid blue line in Figure 5C reveals an increase of the number of (111) defect sites of type P1/P1′ and a significant reduction of accessible (100) terrace sites for hydrogen/sulfate adsorption respective desorption in the presence of SHINERS NPs. The total charge consumed in the double layer region is reduced by ~15% with respect to the NP-free surface. However, the effect is still rather small as compared to the current response of an electrode, which was not exposed to HER conditioning. The dotted blue line in Figure 5C shows that all characteristic features of an ideal Pt(100)-(1 × 1) electrode in H_2SO_4 are blocked completely.

The voltammogram of a bare Pt(100)-(1 × 1) electrode in 0.1 M $HClO_4$ displays a broad current feature between −0.10 to 0.25 V, which is composed of at least two current peaks labeled P1/P1′ and P2/P2′. This potential region is assigned to hydrogen ad/desorption.[55] The broad peak P4/P4′ in $0.25\ V \le E \le 0.45\ V$ is related to OH-adsorption. The charge consumed in $-0.10\ V \le E \le 0.50\ V$ is estimated as $q = 250\ \mu C\ cm^{-2}$. We observed a reduction of the charging current in the hydrogen- and OH-adsorption regions for a Pt(100) electrode modified with SHINERS NPs, even after extended conditioning in the potential region of HER (blue line in Figure 5D). The total charge in both potential regions decreases by *ca.* 30%. The current response of Pt(100)-(1 × 1) in 0.1 M $HClO_4$ with "as-deposited" SHINERS NPs is similar to observations in 0.1 M H_2SO_4 (dotted blue lines in Figure 5C,D). No anion-specific signature could be extracted.

***In Situ* SHINERS Case Study: Pyridine Adsorption on Au(hkl) and Pt(hkl).** We present in this paragraph an application study of the spectro-electrochemical response of 1 mM pyridine dissolved in 0.1 M $NaClO_4$ in contact with Me(111)-(1 × 1) and Me(100)-(1 × 1), Me = Au and Pt, which demonstrates convincingly the great potential of HER-SHINERS in electrochemical surface-science based studies of nanoscale interfacial phenomena. Pyridine qualifies as an ideal compound for model studies on adsorption, orientation and surface coordination of molecules at electrified solid/liquid interfaces.[56,57] Pyridine was the first molecule used in demonstrating the SERS effect and has been an important probe molecule thereafter to test SERS activity and surface properties of SERS substrates.[1−3,58] However, most of these studies were carried out on roughened or colloidal surfaces and interfaces.[6,10,59] Only very few papers report data on atomically flat, truly single-crystalline surfaces.[60] The approaches chosen use either an attenuated total reflection configuration (ATR)[15,61] or SHINERS NPs as plasmonic antennas, as illustrated in our recent preliminary communication.[20]

Figure 6A shows typical voltammograms of a bare (black line) and a HER-SHINERS-NP-modified Au(111) electrode in 1 mM pyridine/0.1 M $NaClO_4$. The current response of the NP-free gold electrode reveals three characteristic pairs of peaks P1/P1′, P2/P2′ and P3/P3′. P1/P1′ is assigned to the ad/desorption of pyridine with the π-system oriented flat on a negatively charged electrode surface.[57,58,62] The coverage increases at more positive potentials, and a certain fraction appears to assume a tilted N-coordinated orientation at defect sites.[63] This process is proposed to start around P2/P2′. Chronocoulometric measurements by Lipkowski *et al.* suggest that a maximum coverage of 1.4×10^{-10} mol cm^{-2} is reached.[62] Next, and close to the potential of zero charge of the pyridine-covered Au(111) surface ($E_{pzc} \approx 0.13$ V) an adlayer structure transition from planar to N-coordinated vertically standing molecules takes place.[62−64] This process is marked by the current peak P3/P3′ and leads to a π-stacked assembly of pyridine molecules on a positively charged electrode at $E >$ P3/P3′ with $\Gamma = 6.7 \times 10^{-10}$ mol cm^{-2}.[62] We note that within the transition region marked by P3/P3′ a certain tilted orientation with a rather small tilt angle referring to the surface normal forms a stable intermediate adlayer,[64] as indicated by the sharp current spikes in $0.10\ V \le E \le 0.20\ V$ in Figure 6A.

The voltammogram of the NP-modified Au(111) electrode (solid blue line in Figure 6A) reproduces the current profile of pyridine adsorption in the double layer region in $-0.70\ V \le E \le 0.05\ V$ and in $0.20\ V \le E \le 0.40\ V$. The charge involved in the structure transition region around P3/P3′ is reduced by *ca.* 30%, and the sharp current spikes are not resolved. Most probably, the SHINERS NPs act as local defects on the electrode surface preventing the formation of a long-range, two-dimensionally ordered adlayer and the phase transition accompanied with it.

The simultaneously recorded SHINERS spectra of pyridine adsorbed on Au(111) are plotted in Figure 6C. Data acquisition started at 0.40 V. We observed four pyridine-related bands, which are assigned to the following A_1 modes: 1009−1012 cm^{-1} (ν_1, ring breathing), 1033−1035 cm^{-1} (ν_{12}, symmetric trigonal ring breathing), 1207−1209 cm^{-1} (ν_{9a}, C−H deformation) and 1593−1597 cm^{-1} (ν_{8a}, ring stretching).[6,10,65−68] The band at 933 cm^{-1}, marked by "*" in Figure 6C, is attributed to coadsorbed perchlorate ions.[24] The pyridine modes are blue-shifted with respect to those in neat pyridine solution. The frequency of the ring breathing mode ν_1 is

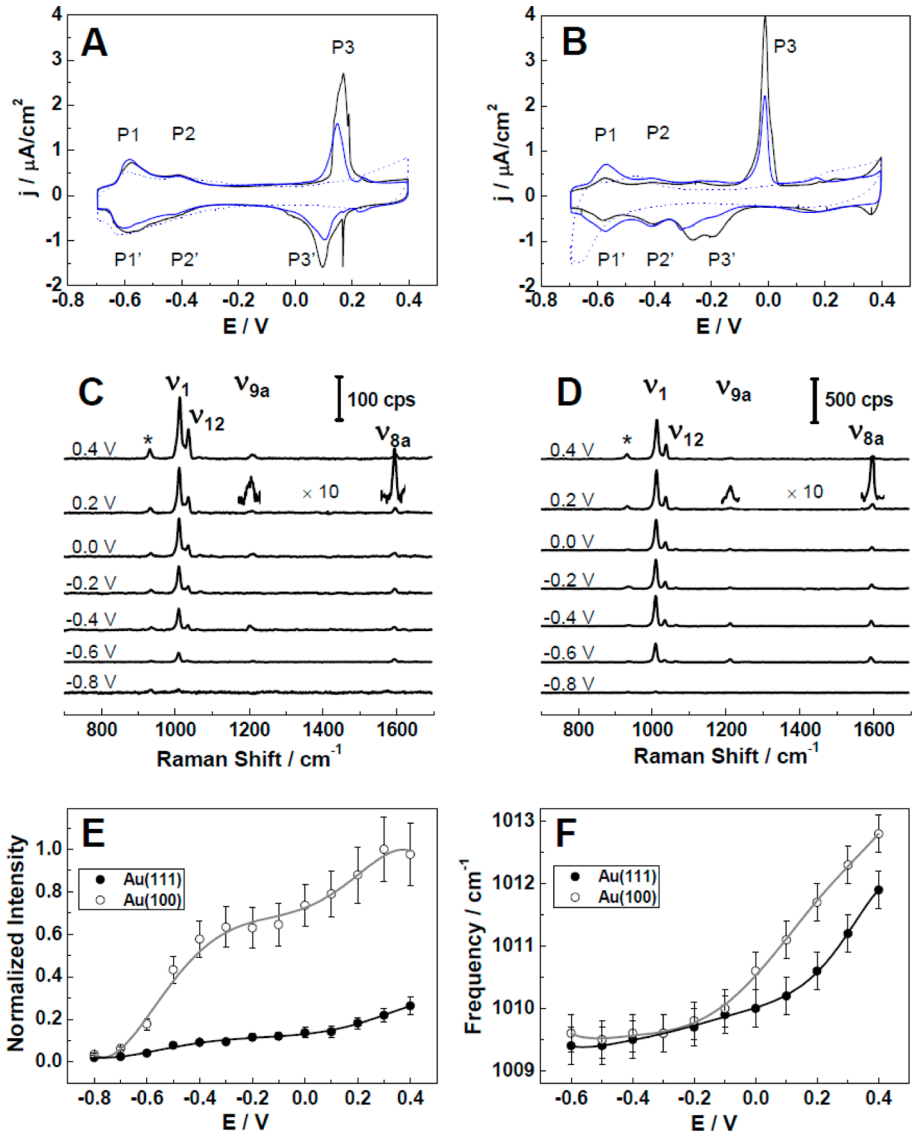

Figure 6. CVs of (A) Au(111)-(1 × 1) and (B) Au(100)-(1 × 1) single-crystal bead electrodes unmodified (black lines) and modified with Au@SiO_2 SHINERS NPs. The dotted blue traces were recorded with "as-prepared" NPs, while the solid blue lines represent data obtained with HER-SHINERS NPs. Solution: 1 mM Py + 0.1 M $NaClO_4$. Scan rate: 10 mV/s. *In situ* SHINER spectra of pyridine adsorbed on (C) Au(111) and (D) Au(100) single-crystal electrode surfaces. Laser power: 1 mW; Collecting time: 10 s. (E) Normalized Raman intensities and (F) Raman frequencies of the ring breathing mode ν_1 in dependence on the applied potentials.

particularly sensitive to potential-dependent structure changes of the pyridine adlayer including electrostatic effects, σ-donation and π-back-donation *etc.*[66−68] Figure 6E,F displays the potential dependence of integrated intensity and peak position of the ν_1 mode. We note that the Raman spectra plotted in Figure 6 are typical data of the HER-SHINERS NPs modified surfaces. Our preparation procedure guarantees a rather uniform size distribution of islands containing 15−20 NPs (see Supporting Information for a characteristic histogram), which can be identified and localized with the help of the CCD-camera of the spectrometer. Typically, we recorded the SHINERS intensity of up to 20 distinct island sites. Employing our preparation procedure of submonolayer HER-SHINERS NPs, we observed a variation in intensity of less than 15%.

We also notice that the SHINERS signal is dominated by contributions from the NP/substrate interface (see FDTD simulations in ref 19), where the pyridine adlayer is well established on unperturbed terrace sites. In consequence, one should expect a strong correlation between the spectroscopic data and other surface electrochemical studies, such as chronocoulometry[62] and cyclic voltammetry. And indeed, the following characteristics were obtained (Figure 6): The ν_1 mode appears with the onset of pyridine adsorption at $E \geq -0.60$ V and grows until −0.40 V, where a first plateau is reached. The corresponding region in the voltammogram is marked by the peaks P1/P1′ and P2/P2′. The peak position varies in this potential region less than 1 cm^{-1}, which points to a slight deviation from a fully planar orientation of the π-system. This interpretation

agrees with conclusions from IR-spectroscopy.[63] An additional increase in intensity is observed at $E \geq 0.10$ V, simultaneously with the appearance of the current peak P3/P3′ in the voltammogram. The signal seems to level off at $E \geq 0.40$ V. $\delta\nu_1/\delta E$ is estimated to 6 cm^{-1}/V. This value of the Stark shift is rather typical for molecular adsorption at electrochemical interfaces with a dipole contribution aligned perpendicularly to the electrode surface.[69] All four pyridine-related A_1 modes scale similarly in their potential dependence of peak intensities and wave numbers.

The above SHINERS data demonstrate unambiguously that pyridine is adsorbed already at a negatively charged Au(111) surface in a none-parallel, most probably slightly tilted orientation with respect to the plane surface, and reorients into a fully upright orientation upon pathing the potential of zero charge at $E > 0.10$ V. Possible complications of this behavior due to reformation of the reconstructed Au(111)-(p × √3) surface or gold island formation upon the subsequent lifting of the reconstruction (see Methods section for details) should be of rather little influence since (1) all experiments started with a fully unreconstructed surface at positive potentials and (2) pyridine blocks drastically the potential-induced surface reconstruction, even at rather negative potentials.[70]

Similar spectro-electrochemical properties were also observed with pyridine on Au(100)-(1 × 1) modified with HER-SHINERS NPs (Figure 6B,D−F). The voltammogramms in the absence (solid black line) and in the presence (solid blue line) of NPs coincide in the double layer region in -0.70 V $\leq E \leq -0.30$ V and in 0.10 V $\leq E \leq$ 0.40 V. Chronocoulometric experiments revealed that the pyridine coverage increases from 0 to *ca.* 3.0×10^{-10} mol cm^{-2} gradually in -0.60 V $\leq E \leq E$(P3), and reaches its saturation value 6.0×10^{-10} mol cm^{-2} at $E > E$(P3) in a step-like manner. This coverage is attributed to pyridine molecules adsorbed in a vertical orientation with the nitrogen atom facing the positively charged Au(100)-(1 × 1) surface.[71] Pyridine adsorption seems to facilitate structure changes of the Au(100) surface, such as the reformation of the Au(100)-(hex) reconstruction at sufficiently negative potentials and its lifting toward the Au(100)-(1 × 1) geometry around 0.0 V upon crossing the potential of zero charge ($E_{pzc} = -0.05$ V), which coincides with the position of P3.[41,70−73] The current peak P3 contains charge contribution from both, the reorientation of adsorbed pyridine as well as of the restructuring of the electrode surface.[57,73]

This complex behavior is also reflected in the voltammogram with HER-SHINERS NPs (Figure 6B). The current peak P3 is reduced by 52% (blue line) as compared to the bare (black line) Au(100) surface. The cathodic counter feature P3′ around −0.20 V is quenched. The corresponding SHINERS spectra, as recorded from 0.40 V toward more negative potentials, are displayed in Figure 6D. Qualitatively, we observed the same pyridine-related bands as for Au(111). Figure 6E,F displays, as a representative example, the potential-dependencies of integrated band intensity and position of the symmetric ν_1 breathing mode. Similar to trends for pyridine on Au(111), the Raman intensity increases from the onset of pyridine adsorption at $E \geq -0.60$ V up to a plateau in -0.40 V $\leq E \leq -0.10$ V, and subsequently raises further in the transition region P3/P3′ until saturation at $E \geq 0.30$ V. The position of the ν_1-mode changes gradually with potential in -0.60 V $\leq E \leq -0.10$ V with $\delta\nu/\delta E \approx 1$ cm^{-1}/V and at $E > -0.10$ V with $\delta\nu/\delta E \approx 6$ cm^{-1}/V. The latter Stark shift is the same as for pyridine/Au(111) at a positively charged electrode. The detection of the ν_1 mode as well as the other pyridine-related modes at $E < E_{pzc}$ and their evolution in dependence on the applied potential demonstrate that pyridine is adsorbed on the negatively charged Au(100) surface in a tilted orientation with the nitrogen atom directed toward the surface and undergoes a structure transition in a N-coordinated vertical adsorption geometry at $E > E$(P3), where the electrode surface bears a positive charge. The data in Figure 6E,F also demonstrate that this transition occurs at more negative potentials on Au(100)-(1 × 1) as compared to Au(111)-(1 × 1). This trend correlates with the more negative value of E_{pzc} of the former.

Finally, we comment on the higher integrated intensity of the pyridine-related Raman bands on Au(100). We have shown in a previous communication,[20] on the basis of periodic DFT calculations and a theoretical analysis of the dielectric functions, that the facet-dependence is predominantly governed by the dielectric properties of the surface. The much smaller imaginary part of the dielectric function for the (110) plane as compared to the other low-index planes leads to a higher electroreflectance and a much stronger electromagnetic field.

Pyridine adsorption on Pt(111)-(1 × 1) and Pt(100)-(1 × 1) in 0.1 M $NaClO_4$ appears to be less complex as compared to the two gold single-crystal surfaces described above. The voltammograms are displayed in Figure 7A,B. They illustrate that pyridine adsorption starts at potentials $E \geq -0.70$ V, slightly more negative than the onset of hydrogen adsorption and the position of P_1. P_1 is thought to represent the adsorption of neutral pyridine, while features at more negative potentials are attributed tentatively to the protonated form. The pyridine adlayer blocks the adsorption of hydrogen and perchlorate ions, which corroborates with a low double layer charging current (or capacitance) in -0.20 V $\leq E \leq$ 0.30 V. The latter assumes smaller values on Pt(111), which reflects the atomically somewhat larger roughness of the unreconstructed Pt(100)-(1 × 1) surface, as obtained after flame annealing and cooling in an Ar/H_2 atmosphere.[34,44] The voltammograms of pyridine on Pt(111) and Pt(100) in the absence and in the presence of HER-SHINERS NPs superimpose.

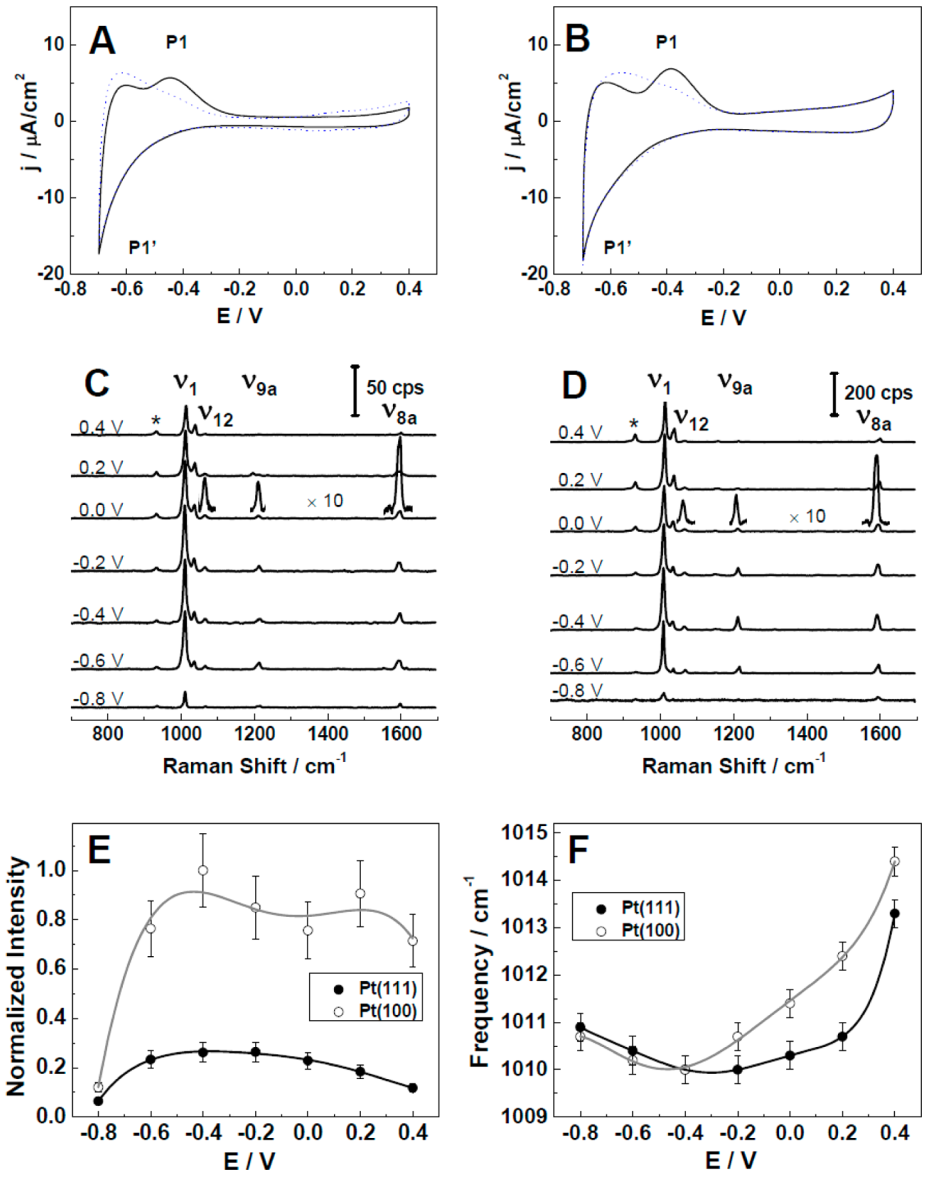

Figure 7. CVs of unmodified (A) Pt(111)-(1 × 1) and (B) Pt(100)-(1 × 1) single-crystal bead electrodes (black lines). The dotted blue traces were recorded with "as-prepared" Au@SiO_2 SHINERS NPs. Solution: 1 mM Py + 0.1 M $NaClO_4$. Scan rate: 50 mV/s. *In situ* SHINER spectra of pyridine adsorbed on (C) Pt(111) and (D) Pt(100) single-crystal electrode surfaces. Laser power: 1 mW. Collecting time: 30 s. (E) Normalized Raman intensities and (F) Raman frequencies of the ring breathing mode ν_1 in dependence on the applied potentials.

The corresponding HER-SHINERS spectra are shown in Figure 7C,D. In addition to the four A_1-modes of pyridine, a fifth band occurs at 1064−1066 cm^{-1}, which is attributed to the C−H deformation A_1-mode ν_{18a}.[66−68] All A_1 modes reveal a similar behavior with increasing electrode potential. Figure 7E,F demonstrates the trend for ν_1. The integrated intensities increase steeply at $E = -0.60$ V and reach a plateau at $E \geq -0.40$ V. The latter decreases slightly at $E \geq 0.20$ V, which is attributed to the onset of competitive adsorption of OH-species.[74] Simultaneously, $\delta\nu_1/\delta E$ increases from 1 cm^{-1}/V at −0.40 V up to 7 cm^{-1}/V at $E > 0.00$ V for both electrodes. These characteristic vibration signatures are interpreted as gradual transfer from an N-coordinated tilted adsorption geometry of pyridine at $E < -0.40$ V to a vertical orientation at $E \geq -0.40$ V. This interpretation is in agreement with conclusions from UHV-transfer experiments at controlled potential and a subsequent analysis of the pyridine adlayer on Pt(111) by Auger electron spectroscopy (AES) and electron energy loss spectroscopy (EELS).[75]

Similar as for pyridine on the two gold facets investigated, the SHINERS signal on Pt(100) is larger as compared to that on Pt(111). This trend is also supported by the different dielectric properties of the two crystallographic orientations.[20]

CONCLUSIONS

We have studied Au(55 nm)@SiO_2 shelled insulated nanoparticles on four low-index phases of gold and

platinum Clavilier-type single-crystal bead electrodes by both electrochemical methods and *in situ* Raman spectroscopy. We demonstrated that Au(hkl) and Pt(hkl) surfaces modified with a submonolayer (and more!) of "as-prepared" SHINERS nanoparticles show distorted voltammetric and spectroscopic responses (see Supporting Information). The electrode surfaces are blocked with surfactants originating from the synthesis of the Au(55 nm)@SiO_2 nanoparticles, which give rise to additional current and spectroscopic features, and therefore cause artifacts in data interpretation and assignment.

We developed an efficient strategy to overcome this problem. Our approach is based on the treatment of surfaces modified with SHINERS NPs in the potential region of hydrogen evolution in 0.1 M aqueous $NaClO_4$. Case studies with Me(111)-(1 × 1) and Me(100)-(1 × 1), Me = Au, Pt, demonstrate the efficiency of our method. Voltammetric experiments in 0.1 M H_2SO_4 and 0.1 M $HClO_4$ reveal that all characteristic double layer features of Au(111) and Au(100) electrodes in contact with these electrolytes coincide in the absence as well as in the presence of the HER-SHINERS NPs. Rather good agreement was also obtained with Pt(111)-(1 × 1) electrodes in both electrolytes. In case of Pt(100)-(1 × 1), qualitative agreement is reached; however, the hydrogen and anion adsorption regions are slightly blocked by the presence of the HER-SHINERS NPs, even after extended cycles of HER treatment. Application studies with these electrodes require some caution and careful control experiments.

Pyridine adsorption and phase formation on Me-(111)-(1 × 1) and Me(100)-(1 × 1), Me = Au, Pt, were chosen as a case study to demonstrate the potential of HER-SHINERS for *in situ* investigations of nanoscale phenomena and processes at electrified solid/liquid interfaces. We obtained high-quality Raman spectra on these well-defined and structurally carefully characterized Au(hkl) and Pt(hkl) single-crystal surfaces. The analysis of the characteristic A_1 vibrational modes revealed perfect agreement with the interpretation of single-crystal voltammetric and chronoamperometric experiments. Our study demonstrates convincingly that the SHINERS protocol as developed in this study qualifies this unique Raman method as a highly promising approach for *in situ* structure and reactivity studies at well-defined electrochemical solid/liquid interfaces. The study also reveals the need of combining the spectro-electrochemical investigations with morphology studies of the respective substrate surface and control experiments on the inertness of the plasmonic nanoparticles with respect to the process under investigation.

METHODS

Chemicals. Chloroauric acid, (3-aminopropyl)trimethoxysilane (97 *M*%; *M*% = mass %), sodium citrate (99 *M*%) and sodium perchlorate (98−100 *M*%) were purchased from Alfa Aesar; sodium silicate solution (27 *M*% SiO_2) and pyridine (≥99.8 *M*%), were obtained from Sigma Aldrich; hydrochloric acid (30%) and suprapure sulfuric acid (96 *M*%) were purchased from Merck. All chemicals were used as received. Water was purified with a Milli-Q system (18.2 MΩ cm, 2−3 ppb total organic content) before use.

Preparation of Au NPs. 55 nm Au NPs were prepared according to the standard sodium citrate reduction method.[76] Briefly, 200 mL of 0.294 mM chloroauric acid were placed in a round-bottom flask and brought to boiling. Next, 1.4 mL of 38.8 mM sodium citrate was added quickly to the boiling solution. The mixture was refluxed for 40 min and then allowed to cool to room temperature.

Preparation of Au@SiO_2 (SHINERS) NPs. Au@SiO_2 SHINERS NPs were prepared by placing 30 mL of the gold NPs solution into a round-bottom flask, adding 0.4 mL of 1 mM (3-aminopropyl-)trimethoxysilane, and stirring for 15 min at room temperature. Next, a 27 *M*% sodium silicate solution was diluted to 0.54 *M*% (∼90.0 mM) and adjusted to pH ∼10.3 with hydrochloric acid. 3.2 mL of the diluted and acidified sodium silicate solution were then added to the reaction mixture, which was stirred afterward at room temperature for 3 more min. The solution was then transferred to a 90 °C bath and stirred for a certain period of time. The shell thickness could be tuned from a few nanometers to tens of nanometers by controlling the reaction time. For example, 30 min or 1 h of heating time resulted in coating the gold core with a layer of about 3 or 5 nm thickness, respectively.[18,33] In this paper, we controlled the reaction time to 30 min, which leads to a silica shell thickness of ∼3 nm (see Figure 1A). The shell is pinhole-free and provides a sufficiently strong enhancement of the pyridine-related Raman signals. Electrochemical and Raman experiments were carried out to ensure that the as-prepared SHINERS NPs are free of pinholes. The test protocols were described in our previous papers.[18,19,24]

The hot NP mixture was then transferred into test tubes of 1.5 mL volume and cooled down in an ice bath, which quenches the reaction. Upon cooling down to room temperature, the samples were centrifuged at 5500 rpm for 15 min. The supernatant was removed afterward. The concentrated SHINERS NPs at the bottom of the test tube were diluted and centrifuged again. This procedure was repeated several times. The cleaned Au@SiO_2 NPs were dissolved in 200 μL of Milli-Q water, which leads to a solution containing ∼1.97 mM total gold. Two microliters of this solution were then casted onto a freshly prepared Au(hkl) or Pt(hkl) single-crystal bead electrode (Figure 1B) and subsequently dried in a gentle stream of argon. The SHINERS NPs form a submonolayer of small, statistically distributed two-dimensional islands, which contain typically 15−20 NPs. The NP-coverage as obtained from SEM and AFM measurements (Figure 1) is estimated to range between 20 to 30%. We note that the silicon shell prevents the formation of three-dimensional aggregates.

Preparation of Au(hkl) and Pt(hkl) Single-Crystal Electrodes. The electrodes used were Clavilier-type half-bead single-crystal Au(hkl) and Pt(hkl) electrodes (∼ 2 mm diameter, Figure 1B). Island-free and unreconstructed Au(hkl)-(1 × 1) electrodes were prepared according to a previously described procedure.[40] Briefly, the electrode was annealed in a butane flame for about 2 min and cooled down to room temperature in an argon atmosphere. The flame-annealed Au(hkl) electrode was then immersed into 10 mM HCl at open circuit for 10 min to lift the reconstruction, which leads to island-free Au(hkl)-(1 × 1) surfaces with rather large terraces. The chloride ions were removed by extended rinsing with Milli-Q water. The electrode was finally dried in a stream of argon.

The Pt(hkl) electrodes were annealed in a hydrogen flame for 1 min. The hot electrodes were quickly transferred into a closed flask filled with a mixture of Ar/H_2 (4:1) and allowed to

cool down to room temperature. The procedure leads to the lifting of the surface reconstruction.[34,44] Flow and composition of the gases in the flask were adjusted to ensure a slow cooling rate. The cooled electrode was subsequently immersed into deaerated Milli-Q water, which was saturated with hydrogen, and then transferred with a protecting droplet of water adhering to the polished surface into the electrochemical cell for further characterization and/or modification.

Cyclic Voltammetry. The electrochemical measurements were conducted in a three compartment all-glass cell with a platinum or gold coil as auxiliary electrode and a leakless Ag/AgCl reference electrode in 0.1 M $NaClO_4$ or a trapped, reversible hydrogen reference electrode (RHE) in 0.1 M H_2SO_4 and $HClO_4$, respectively. High-purity Ar (Alphagaz 99.999%) was employed to deaerate the solutions. Ar was also passed above the solutions during the experiments. The freshly prepared electrodes were brought in contact with the electrolyte under potential control in a hanging meniscus configuration. The electrochemical measurements were carried out with an Autolab PGSTAT30.

Raman Spectroscopy. Raman spectra were recorded with a LabRam HR800 confocal microprobe Raman system (HORIBA Jobin Yvon). The excitation wavelength was 632.8 nm from a He−Ne laser. The power on the sample was typically about 1 mW. A 50× magnification long-working-distance objective (8 mm) was used to focus the laser onto the sample and to collect the scattered light in a backscattering geometry. A lab-made spectro-electrochemical cell with a Pt or a Au wire and an Ag/AgCl electrode serving as the counter and the reference electrodes was used for the electrochemical SERS measurements (Figure 3A). All *in situ* Raman experiments were carried out in the strict absence of oxygen. The simultaneous electrochemical control was achieved by employing a lab-built potentiostat and software developed in our group.

Conflict of Interest: The authors declare no competing financial interest.

Acknowledgment. The authors acknowledge support from the Swiss National Science Foundation SNF under 200021-124643, NRP 62, and the FP7 NMP Project BACWIRE.

Supporting Information Available: Size-distribution of HER-SHINERS NP islands, SHINERS spectra of Py on Au(111) and Pt(111) with and without HER cleaning procedure, and surface enhancement factor (SEF) calculation. This material is available free of charge *via* the Internet at http://pubs.acs.org.

REFERENCES AND NOTES

1. Fleischmann, M.; Hendra, P. J.; McQuillan, A. J. Raman Spectra of Pyridine Adsorbed at a Silver Electrode. *Chem. Phys. Lett.* **1974**, *26*, 163–166.
2. Jeanmaire, D. L.; Vanduyne, R. P. Surface Raman Spectroelectrochemistry. 1. Heterocyclic, Aromatic, and Aliphatic Amines Adsorbed on Anodized Silver Electrode. *J. Electroanal. Chem.* **1977**, *84*, 1–20.
3. Albrecht, M. G.; Creighton, J. A. Anomalously Intense Raman-Spectra of Pyridine at a Silver Electrode. *J. Am. Chem. Soc.* **1977**, *99*, 5215–5217.
4. Ren, B.; Liu, G. K.; Lian, X. B.; Yang, Z. L.; Tian, Z. Q. Raman Spectroscopy on Transition Metals. *Anal. Bioanal. Chem.* **2007**, *388*, 29–45.
5. Tian, Z. Q.; Ren, B.; Li, J. F.; Yang, Z. L. Expanding Generality of Surface-Enhanced Raman Spectroscopy with Borrowing SERS Activity Strategy. *Chem. Commun.* **2007**, 3514–3534.
6. Wu, D. Y.; Li, J. F.; Ren, B.; Tian, Z. Q. Electrochemical Surface-Enhanced Raman Spectroscopy of Nanostructures. *Chem. Soc. Rev.* **2008**, *37*, 1025–1041.
7. Kneipp, K.; Moskovits, M.; Kneipp, H. *Surface-Enhanced Raman Scattering Physics and Applications*; Springer: Berlin/Heidelberg, 2006; Vol. 103.
8. Schatz, G. C.; Young, M. A.; Van Duyne, R. P. Electromagnetic Mechanism of SERS. *Top. Appl. Phys.* **2006**, *103*, 19–45.
9. Moskovits, M. Surface-Enhanced Raman Spectroscopy: A Brief Perspective. *Top. Appl. Phys.* **2006**, *103*, 1–17.
10. Creighton, J. A.; Blatchford, C. G.; Albrecht, M. G. Plasma Resonance Enhancement of Raman Scattering by Pyridine Adsorbed on Silver or Gold Sol Particles of Size Comparable to the Excitation Wavelength. *J. Chem. Soc., Faraday Trans. 2* **1979**, *75*, 790–798.
11. Wetzel, H.; Gerischer, H.; Pettinger, B. Comparison of the Potential Dependence of the Surface-Enhanced Raman Effect at Colloid Silver Particles and Bulk Silver Electrodes. *Chem. Phys. Lett.* **1982**, *85*, 187–189.
12. Nikoobakht, B.; Wang, J. P.; El-Sayed, M. A. Surface-Enhanced Raman Scattering of Molecules Adsorbed on Gold Nanorods: Off-Surface Plasmon Resonance Condition. *Chem. Phys. Lett.* **2002**, *366*, 17–23.
13. Willets, K. A.; Van Duyne, R. P. Localized Surface Plasmon Resonance Spectroscopy and Sensing. *Annu. Rev. Phys. Chem.* **2007**, *58*, 267–297.
14. Mahajan, S.; Abdelsalam, M.; Suguwara, Y.; Cintra, S.; Russell, A.; Baumberg, J.; Bartlett, P. Tuning Plasmons on Nano-Structured Substrates for NIR-SERS. *Phys. Chem. Chem. Phys.* **2007**, *9*, 104–109.
15. Bruckbauer, A.; Otto, A. Raman Spectroscopy of Pyridine Adsorbed on Single Crystal Copper Electrodes. *J. Raman Spectrosc.* **1998**, *29*, 665–672.
16. Ikeda, K.; Suzuki, S.; Uosaki, K. Crystal Face Dependent Chemical Effects in Surface-Enhanced Raman Scattering at Atomically Defined Gold Facets. *Nano Lett.* **2011**, *11*, 1716–1722.
17. Cui, L.; Liu, B.; Vonlanthen, D.; Mayor, M.; Fu, Y. C.; Li, J. F.; Wandlowski, T. *In-Situ* Gap-Mode Raman Spectroscopy on Single-Crystal Au(100) Electrodes: Tuning the Torsion Angle of 4,4′-Biphenyldithiols by an Electrochemical Gate Field. *J. Am. Chem. Soc.* **2011**, *133*, 7332–7335.
18. Li, J. F.; Huang, Y. F.; Ding, Y.; Yang, Z. L.; Li, S. B.; Zhou, X. S.; Fan, F. R.; Zhang, W.; Zhou, Z. Y.; Wu, D. Y.; *et al.* Shell-Isolated Nanoparticle-Enhanced Raman Spectroscopy. *Nature* **2010**, *464*, 392–395.
19. Anema, J. R.; Li, J. F.; Yang, Z. L.; Ren, B.; Tian, Z. Q. Shell-Isolated Nanoparticle-Enhanced Raman Spectroscopy: Expanding the Versatility of Surface-Enhanced Raman Scattering. *Annu. Rev. Anal. Chem.* **2011**, *4*, 129–150.
20. Li, J. F.; Ding, S. Y.; Yang, Z. L.; Bai, M. L.; Anema, J. R.; Wang, X.; Wang, A.; Wu, D. Y.; Ren, B.; Hou, S. M.; *et al.* Extraordinary Enhancement of Raman Scattering from Pyridine on Single Crystal Au and Pt Electrodes by Shell-Isolated Au Nanoparticles. *J. Am. Chem. Soc.* **2011**, *133*, 15922–15925.
21. Uzayisenga, V.; Lin, X. D.; Li, L. M.; Anema, J. R.; Yang, Z. L.; Huang, Y. F.; Lin, H. X.; Li, S. B.; Li, J. F.; Tian, Z. Q. Synthesis, Characterization, and 3D-FTDT Simulation of Ag@SiO_2 Nanoparticles for Shell-Isolated Nanoparticle-Enhanced Raman Spectroscopy. *Langmuir* **2012**, *28*, 9140–9146.
22. Pettinger, B.; Schambach, P.; Villagomez, C. J.; Scott, N. Tip-Enhanced Raman Spectroscopy: Near-Fields Acting on a Few Molecules. *Annu. Rev. Phys. Chem.* **2012**, *63*, 379–399.
23. Schmid, T.; Yeo, B. S.; Leong, G.; Stadler, J.; Zenobi, R. Performing Tip-Enhanced Raman Spectroscopy in Liquids. *J. Raman Spectrosc.* **2009**, *40*, 1392–1399.
24. Liu, B.; Blaszczyk, A.; Mayor, M.; Wandlowski, T. Redox-Switching in a Viologen-Type Adlayer: An Electrochemical Shell-Isolated Nanoparticle Enhanced Raman Spectroscopy Study on Au(111)-(1 × 1) Single Crystal Electrodes. *ACS Nano* **2011**, *5*, 5662–5672.
25. Butcher, D. P.; Boulos, S. P.; Murphy, C. J.; Ambrosio, R. C.; Gewirth, A. A. Face-Dependent Shell-Isolated Nanoparticle Enhanced Raman Spectroscopy of 2,2′-Bipyridine on Au(100) and Au(111). *J. Phys. Chem. C* **2012**, *116*, 5128–5140.
26. Honesty, N. R.; Gewirth, A. A. Shell-Isolated Nanoparticle Enhanced Raman Spectroscopy (Shiners) Investigation of Benzotriazole Film Formation on Cu(100), Cu(111), and Cu(Poly). *J. Raman Spectrosc.* **2012**, *43*, 46–50.
27. Zhumaev, U.; Rudnev, A. V.; Li, J. F.; Kuzume, A.; Vu, T. H.; Wandlowski, T. Electro-Oxidation of Au(111) in Contact with Aqueous Electrolytes: New Insight from *in-Situ* Vibration Spectroscopy. *Electrochim. Acta* **2013**, 10.1016/j.electacta.2013.02.105.

28. Attard, G.; Bennett, J. A.; Mikheenko, I.; Jenkins, P.; Guan, S.; Macaskie, L. E.; Wood, J.; Wain, A. J. Semi-Hydrogenation of Alkynes at Single Crystal, Nanoparticle and Biogenic Nanoparticle Surfaces: The role of Defects in Lindlar-Type Catalysts and the Origin of their Selectivity. *Faraday Discuss.* **2013**, *62*, 57–75.
29. Li, M. D.; Cui, Y.; Gao, M. X.; Luo, J.; Ren, B.; Tian, Z. Q. Clean Substrates Prepared by Chemical Adsorption of Iodide Followed by Electrochemical Oxidation for Surface-Enhanced Raman Spectroscopic Study of Cell Membrane. *Anal. Chem.* **2008**, *80*, 5118–5125.
30. Bewick, A.; Thomas, B. Optical and Electrochemical Studies of Underpotential Deposition of Metals 1: Thallium Deposition on Single-Crystal Silver Electrodes. *J. Electroanal. Chem.* **1975**, *65*, 911–931.
31. Taylor, C. E.; Garvey, S. D.; Pemberton, J. E. Carbon Contamination at Silver Surfaces: Surface Preparation Procedures Evaluated by Raman Spectroscopy and X-Ray Photoelectron Spectroscopy. *Anal. Chem.* **1996**, *68*, 2401–2408.
32. Vidal-Iglesias, F. J.; Solla-Gullon, J.; Herrero, E.; Montiel, V.; Aldaz, A.; Feliu, J. M. Evaluating the Ozone Cleaning Treatment in Shape-Controlled Pt Nanoparticles: Evidences of Atomic Surface Disordering. *Electrochem. Commun.* **2011**, *13*, 502–505.
33. Li, J. F.; Li, S. B.; Anema, J. R.; Yang, Z. L.; Huang, Y. F.; Ding, Y.; Wu, Y. F.; Zhou, X. S.; Wu, D. Y.; Ren, B.; *et al.* Synthesis and Characterization of Gold Nanoparticles Coated with Ultrathin and Chemically Inert Dielectric Shells for SHINERS Applications. *Appl. Spectrosc.* **2011**, *65*, 620–626.
34. Kibler, L. A. *Preparation and Characterization of Noble Metal Single Crystal Electrode Surfaces*; ISE: Barcelona, 2003.
35. Clavilier, J. Flame-Annealing and Cleaning Technique. In *Interfacial Electrochemistry: Theory, Experimental, and Applications*; Wieckowski, A., Ed.; Marcel Dekker: New York, 1999; pp 231−248.
36. Clavilier, J.; Faure, R.; Guinet, G.; Durand, R. Preparation of Mono-Crystalline Pt Microelectrodes and Electrochemical Study of the Plane Surfaces Cut in the Direction of the (111) and (110) Planes. *J. Electroanal. Chem.* **1980**, *107*, 205–209.
37. Clavilier, J. Role of Anion on the Electrochemical-Behavior of a (111) Platinum Surface—Unusual Splitting of the Voltammogram in the Hydrogen Region. *J. Electroanal. Chem.* **1980**, *107*, 211–216.
38. Angerstein-Kozlowska, H.; Conway, B. E.; Hamelin, A.; Stoicoviciu, L. Elementary Steps of Electrochemical Oxidation of Single-Crystal Planes of Au 1: Chemical Basis of Processes Involving Geometry of Anions and the Electrode Surfaces. *Electrochim. Acta* **1986**, *31*, 1051–1061.
39. Angerstein-Kozlowska, H.; Conway, B. E.; Hamelin, A.; Stoicoviciu, L. Elementary Steps of Electrochemical Oxidation of Single-Crystal Planes of Au 2: A Chemical and Structural Basis of Oxidation of the (111) Plane. *J. Electroanal. Chem.* **1987**, *228*, 429–453.
40. Holzle, M. H.; Wandlowski, T.; Kolb, D. M. Phase-Transition in Uracil Adlayers on Electrochemically Prepared Island-Free Au(100)-(1 × 1). *J. Electroanal. Chem.* **1995**, *394*, 271–275.
41. Kolb, D. M. Reconstruction Phenomena at Metal-Electrolyte Interfaces. *Prog. Surf. Sci.* **1996**, *51*, 109–173.
42. Dakkouri, A. S.; Kolb, D. M. Reconstruction of Gold Surfaces. In *Interfacial Electrochemistry*; Wieckowski, A., Ed.; Marcel-Dekker: New York, 1999; pp 151−173.
43. Dretschkow, T.; Wandlowski, T. In *Topics in Applied Physics*; Wandelt, K., Thurgate, S., Eds.; Springer: Berlin, 2003; Vol. 85, pp 259−321.
44. Rudnev, A. V.; Wandlowski, T. An Influence of Pretreatment Conditions on Surface Structure and Reactivity of Pt(100) Towards Co Oxidation Reaction. *Russ. J. Electrochem.* **2012**, *48*, 259–270.
45. Scherson, D. A.; Kolb, D. M. Voltammetric Curves for Au(111) in Acid-Media—A Comparison with Pt(111) Surfaces. *J. Electroanal. Chem.* **1984**, *176*, 353–357.
46. Garcia-Araez, N.; Climent, V.; Rodriguez, P.; Feliu, J. M. Thermodynamic Analysis of (Bi)Sulphate Adsorption on a Pt(111) Electrode as a Function of pH. *Electrochim. Acta* **2008**, *53*, 6793–6806.
47. Wagner, F. T.; Ross, P. N. Leed Analysis of Electrode Surfaces—Structural Effects of Potentiodynamic Cycling on Pt Single-Crystals. *J. Electroanal. Chem.* **1983**, *150*, 141–164.
48. Clavilier, J.; Armand, D.; Sun, S. G.; Petit, M. Electrochemical Adsorption Behavior of Platinum Stepped Surfaces in Sulfuric-Acid-Solutions. *J. Electroanal. Chem.* **1986**, *205*, 267–277.
49. Clavilier, J.; Feliu, J. M.; Fernandez-Vega, A.; Aldaz, A. Electrochemical-Behavior of Irreversibly Adsorbed Bismuth on Pt(100) with Different Degrees of Crystalline Surface Order. *J. Electroanal. Chem.* **1989**, *269*, 175–189.
50. Feliu, J. M.; Orts, J. M.; Gomez, R.; Aldaz, A.; Clavilier, J. New Information on the Unusual Adsorption States of Pt(111) in Sulfuric-Acid-Solutions from Potentiostatic Adsorbate Replacement by CO. *J. Electroanal. Chem.* **1994**, *372*, 265–268.
51. Armand, D.; Clavilier, J. Quantitative-Analysis of the Distribution of the Hydrogen Adsorption States at Platinum Surfaces. 1. Application to Pt(100) in Sulfuric-Acid Medium. *J. Electroanal. Chem.* **1987**, *225*, 205–214.
52. Armand, D.; Clavilier, J. Quantitative-Analysis of the Distribution of the Hydrogen Adsorption States at Platinum Surfaces 2: Application to Pt(110), Stepped and Polyoriented Platinum Surfaces in Sulfuric-Acid Medium. *J. Electroanal. Chem.* **1987**, *233*, 251–265.
53. Rodes, A.; Zamakhchari, M. A.; Elachi, K.; Clavilier, J. Electrochemical-Behavior of Pt(100) in Various Acidic Media 1: On a New Voltammetric Profile of Pt(100) in Perchloric-Acid and Effects of Surface-Defects. *J. Electroanal. Chem.* **1991**, *305*, 115–129.
54. Francke, R.; Climent, V.; Baltruschat, H.; Feliu, J. M. Electrochemical Deposition of Copper on Stepped Platinum Surfaces in the 011 Zone Vicinal to the (100) Plane. *J. Electroanal. Chem.* **2008**, *624*, 228–240.
55. Garcia-Araez, N.; Climent, V.; Feliu, J. M. Analysis of Temperature Effects on Hydrogen and OH Adsorption on Pt(111), Pt(100) and Pt(110) by Means of Gibbs Thermodynamics. *J. Electroanal. Chem.* **2010**, *649*, 69–82.
56. Lipkowski, J.; Stolberg, L. Molecular Adsorption at Gold and Silver Electrodes. In *Adsorption of Molecules at Metal Electrodes*; Lipkowski, J., Ross, P. N., Eds.; VCH: New York, 1992; pp 171−238.
57. Lipkowski, J.; Stolberg, L.; Yang, D. F.; Pettinger, B.; Mirwald, S.; Henglein, F.; Kolb, D. M. Molecular Adsorption at Metal Electrodes. *Electrochim. Acta* **1994**, *39*, 1045–1056.
58. Stolberg, L.; Lipkowski, J.; Irish, D. E. An Examination of the Relationship Between Surface Enhanced Raman Scattering (SERS) Intensities and Surface Concentration for Pyridine Adsorbed at the Polycrystalline Gold/Aqueous Solution Interface. *J. Electroanal. Chem.* **1991**, *300*, 563–584.
59. Wetzel, H.; Gerischer, H.; Pettinger, B. Surface Enhanced Raman-Scattering from Silver-Halide and Silver-Pyridine Vibrations and the Role of Silver Ad-Atoms. *Chem. Phys. Lett.* **1981**, *78*, 392–397.
60. Campion, A.; Mullins, D. R. Normal Raman Scattering from Pyridine Adsorbed on the Low-Index Faces of Silver. *Chem. Phys. Lett.* **1983**, *94*, 576–579.
61. Futamata, M. Highly-Sensitive Raman Spectroscopy to Characterize Adsorbates on the Electrode. *Surf. Sci.* **1997**, *386*, 89–92.
62. Stolberg, L.; Morin, S.; Lipkowski, J.; Irish, D. E. Adsorption of Pyridine at the Gold(111)-Solution Interface. *J. Electroanal. Chem.* **1991**, *307*, 241–242.
63. Hoon-Khosla, M.; Fawcett, W. R.; Chen, A. C.; Lipkowski, J.; Pettinger, B. A SNIFTIRS Study of the Adsorption of Pyridine at the Au(111) Electrode-Solution Interface. *Electrochim. Acta* **1999**, *45*, 611–621.
64. Cai, W. B.; Wan, L. J.; Noda, H.; Hibino, Y.; Ataka, K.; Osawa, M. Orientational Phase Transition in a Pyridine Adlayer on Gold(111) in Aqueous Solution Studied by *in-Situ* Infrared Spectroscopy and Scanning Tunneling Microscopy. *Langmuir* **1998**, *14*, 6992–6998.

65. Wu, D. Y.; Ren, B.; Jiang, Y. X.; Xu, X.; Tian, Z. Q. Density Functional Study and Normal-Mode Analysis of the Bindings and Vibrational Frequency Shifts of the Pyridine-M (M = Cu, Ag, Au, Cu^+, Ag^+, Au^+, and Pt) Complexes. *J. Phys. Chem. A* **2002**, *106*, 9042–9052.
66. Wu, D. Y.; Liu, X. M.; Duan, S.; Xu, X.; Ren, B.; Lin, S. H.; Tian, Z. Q. Chemical Enhancement Effects in Sers Spectra: A Quantum Chemical Study of Pyridine Interacting with Copper, Silver, Gold and Platinum Metals. *J. Phys. Chem. C* **2008**, *112*, 4195–4204.
67. Wu, D. Y.; Hayashi, M.; Lin, S. H.; Tian, Z. Q. Theoretical Differential Raman Scattering Cross-Sections of Totally-Symmetric Vibrational Modes of Free Pyridine and Pyridine-Metal Cluster Complexes. *Spectrochim. Acta A* **2004**, *60*, 137–146.
68. Zhao, L. L.; Jensen, L.; Schatz, G. C. Pyridine-Ag-20 Cluster: A Model System for Studying Surface-Enhanced Raman Scattering. *J. Am. Chem. Soc.* **2006**, *128*, 2911–2919.
69. Wasileski, S. A.; Koper, M. T. M.; Weaver, M. J. Field-Dependent Electrode-Chemisorbate Bonding: Sensitivity of Vibrational Stark Effect and Binding Energetics to Nature of Surface Coordination. *J. Am. Chem. Soc.* **2002**, *124*, 2796–2805.
70. Hamm, U. W.; Kolb, D. M. On the Stability of Reconstructed Au(100) Surfaces in the Presence of Organic-Molecules. *J. Electroanal. Chem.* **1992**, *332*, 339–347.
71. Stolberg, L.; Lipkowski, J.; Irish, D. E. Adsorption of Pyridine at the Gold(100)-Solution Interface. *J. Electroanal. Chem.* **1987**, *238*, 333–353.
72. Wu, S.; Lipkowski, J.; Magnussen, O. M.; Ocko, B. M.; Wandlowski, T. The Driving Force for $(p \times \sqrt{3})<->(1 \times 1)$ Phase Transition of Au(111) in the Presence of Organic Adsorption: A Combined Chronocoulometric and Surface X-Ray Scattering Study. *J. Electroanal. Chem.* **1998**, *446*, 67–77.
73. Skoluda, P.; Holzle, M.; Lipkowski, J.; Kolb, D. M. Pyridine Adsorption on Reconstructed and Unreconstructed Au-(100). *J. Electroanal. Chem.* **1993**, *358*, 343–349.
74. Conway, B. E. Electrochemical Oxide Film Formation at Noble-Metals as a Surface-Chemical Process. *Prog. Surf. Sci.* **1995**, *49*, 331–452.
75. Stern, D. A.; Lagurendavidson, L.; Frank, D. G.; Gui, J. Y.; Lin, C. H.; Lu, F.; Salaita, G. N.; Walton, N.; Zapien, D. C.; Hubbard, A. T. Potential-Dependent Surface-Chemistry of 3-Pyridinecarboxylic Acid (Niacin) and Related-Compounds at Pt(111) Electrodes. *J. Am. Chem. Soc.* **1989**, *111*, 877–891.
76. Frens, G. Controlled Nucleation for Regulation of Particle-Size in Monodisperse Gold Suspensions. *Nature (London), Phys. Sci.* **1973**, *241*, 20–22.